The Astrophysical Journal, 909:30 (15pp), 2021 March 1 https://doi.org/10.3847/1538-4357/abe045

StrayCats: A Catalog of NuSTAR Stray Light Observations

Brian W. Grefenstette[1], Renee M. Ludlam[1,10], Ellen T. Thompson[2], Javier A. García[1,3], Jeremy Hare[4,11], Amruta D. Jaodand[1], Roman A. Krivonos[5], Kristin K. Madsen[6,7], Guglielmo Mastroserio[1], Catherine M. Slaughter[8,12], John A. Tomsick[2], Daniel Wik[9], and Andreas Zoglauer[2]
[1] Cahill Center for Astronomy and Astrophysics, California Institute of Technology, Pasadena, CA 91125, USA; bwgref@srl.caltech.edu
[2] Space Sciences Laboratory, 7 Gauss Way, University of California, Berkeley, CA 94720-7450, USA
[3] Dr. Karl Remeis-Observatory and Erlangen Centre for Astroparticle Physics, Sternwartstr. 7, D-96049 Bamberg, Germany
[4] NASA Goddard Space Flight Center, Greenbelt, MD 20771, USA
[5] Space Research Institute, Russian Academy of Sciences, Profsoyuznaya 84/32, 117997 Moscow, Russia
[6] Space Radiation Laboratory, Caltech, 1200 East California Boulevard, Pasadena, CA 91125, USA
[7] CRESST and X-ray Astrophysics Laboratory, NASA Goddard Space Flight Center, Greenbelt, MD 20771, USA
[8] Department of Physics and Astronomy, Dartmouth College, 6127 Wilder Laboratory, Hanover, NH 03755, USA
[9] Department of Physics and Astronomy, University of Utah, 201 James Fletcher Building, Salt Lake City, UT 84112, USA
Received 2020 November 13; revised 2021 January 18; accepted 2021 January 25; published 2021 March 3

Abstract

We present `StrayCats`, a catalog of NuSTAR stray light observations of X-ray sources. Stray light observations arise for sources 1°–4° away from the telescope pointing direction. At this off-axis angle, X-rays pass through a gap between the optics and aperture stop and so do not interact with the X-ray optics; instead, they directly illuminate the NuSTAR focal plane. We have systematically identified and examined over 1400 potential observations resulting in a catalog of 436 telescope fields and 78 stray light sources that have been identified. The sources identified include historically known persistently bright X-ray sources, X-ray binaries in outburst, pulsars, and type I X-ray bursters. In this paper, we present an overview of the catalog, how we identified the `StrayCats` sources, and the analysis techniques required to produce high-level science products. Finally, we present a few brief examples of the science quality of these unique data.

Unified Astronomy Thesaurus concepts: X-ray surveys (1824); Astrophysical black holes (98); Neutron stars (1108); High mass x-ray binary stars (733); Low-mass x-ray binary stars (939); Pulsars (1306)

1. Introduction

Compact objects in our galaxy provide an excellent laboratory in which to study matter in extreme conditions. Of most interest are neutron stars (NSs) and black holes (BHs) in binary systems, where the compact object accretes material from its companion star either through Roche lobe overflow or through a stellar wind from the companion. The inflowing material forms an accretion disk around the compact object with temperatures hot enough to produce copious amounts of thermal X-rays and giving rise to a corona of nonthermal electrons emitting in the hard X-ray band.

The hard X-ray ($E \geqslant 3$ keV) bandpass provides essential diagnostic information on the accretion state of the source and clues to the nature of the compact object in the system. The high-energy ($E \geqslant 20$ keV) spectrum of the X-ray binaries in the Galactic plane has been surveyed with low spectral resolution instruments on the INTErnational Gamma-Ray Astrophysics Laboratory (INTEGRAL; Winkler et al. 2003) and the Neil Gehrels Swift Observatory (Gehrels et al. 2004).

Targeted observations with the Nuclear Spectroscopic Telescope ARray (NuSTAR; Harrison et al. 2013) have demonstrated the diagnostic power of a sensitive instrument over the 3–80 keV bandpass. However, when these sources go into an X-ray bright state, they result in extremely high count rates and correspondingly high telemetry loads. Because of this, many observations of bright sources are short in duration (≈20 ks) to allow the spacecraft to transmit the data down to the ground without overwriting the storage drives on board. Unlike Swift, NuSTAR is not a rapidly slewing instrument, so repeated short monitoring observations of the same target are not generally possible due to scheduling constraints and require "target of opportunity" (ToO) programs that can take days or a week to get on target once an observation is triggered.

Fortunately, NuSTAR can also serendipitously observe bright X-ray binaries through "stray light." While NuSTAR is well known as the first focusing hard X-ray satellite in orbit, the open geometry of the mast that connects the optics to the detectors allows for the possibility of stray light (light that has not been focused by the optics) illuminating detectors. This is typically referred to as "aperture flux," since the light passes through the open area of the aperture stops (see Figure 1) and occurs for sources that are roughly 1°–4° from the center of the NuSTAR field of view (FoV; Madsen et al. 2017a).

For most NuSTAR observations, the dominant source of aperture X-ray emission is the cosmic X-ray background (hereafter "aperture" CXB, or aCXB). This is the superposition of X-ray light from a uniform background of (unresolved) active galactic nuclei (AGN) in the 1°–4° annulus. This contribution to the NuSTAR background has been well documented (e.g., Wik et al. 2014) and is generally described by a spatial gradient in the NuSTAR background across the FoV.

When stray light comes from a single off-axis source, the emission geometry is much simpler. Instead of a "gradient" in the background, we instead observe an easily identified shadow of the aperture stop ring sharply cutting off the source (Figure 2). Because the X-rays do not interact with the NuSTAR optics, the response of the instrument is somewhat

[10] NASA Einstein Fellow.
[11] NASA Postdoctoral Program Fellow.
[12] Caltech Summer Undergraduate Research Fellowship.

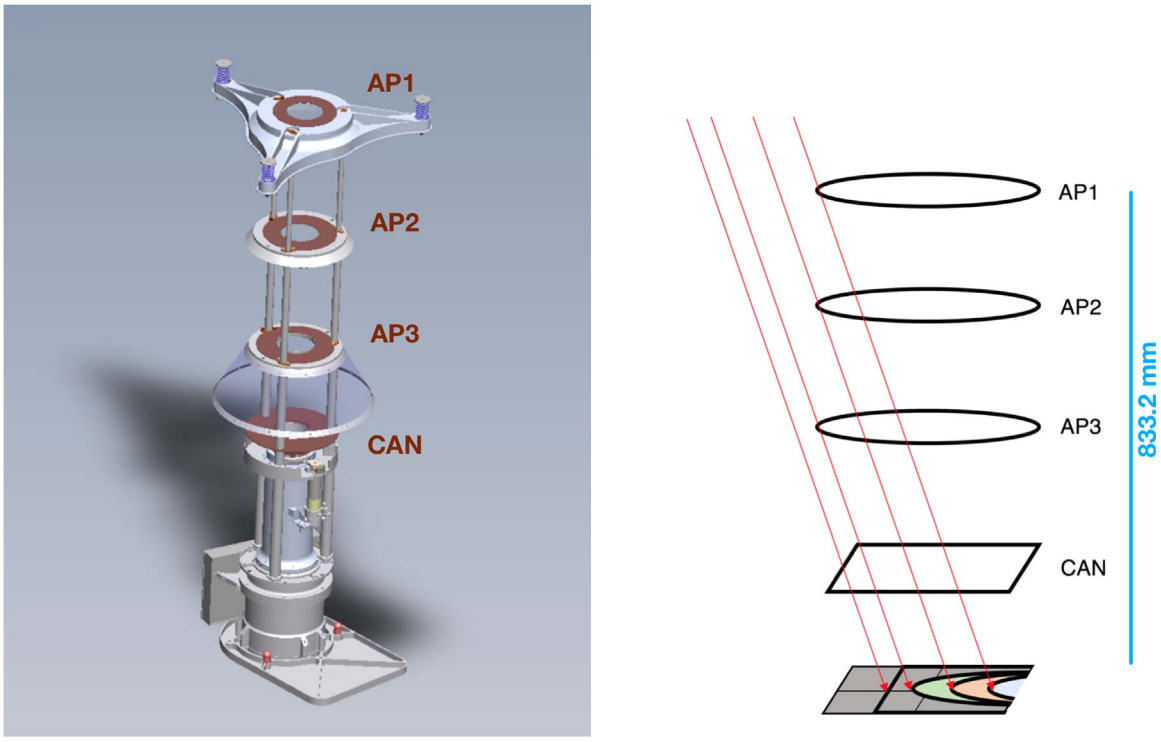

Figure 1. Schematic of the path of stray light photons. (Left) CAD rendering of the focal plane and aperture stop assembly. (Right) Red lines show the stray light paths that survive to the focal plane after passing around the aperture stop (AP1, AP2, and AP3) rings and the "can" housing the detectors. The height offset from the focal plane to AP1 is shown on the right. Figures adapted from Madsen et al. (2017a).

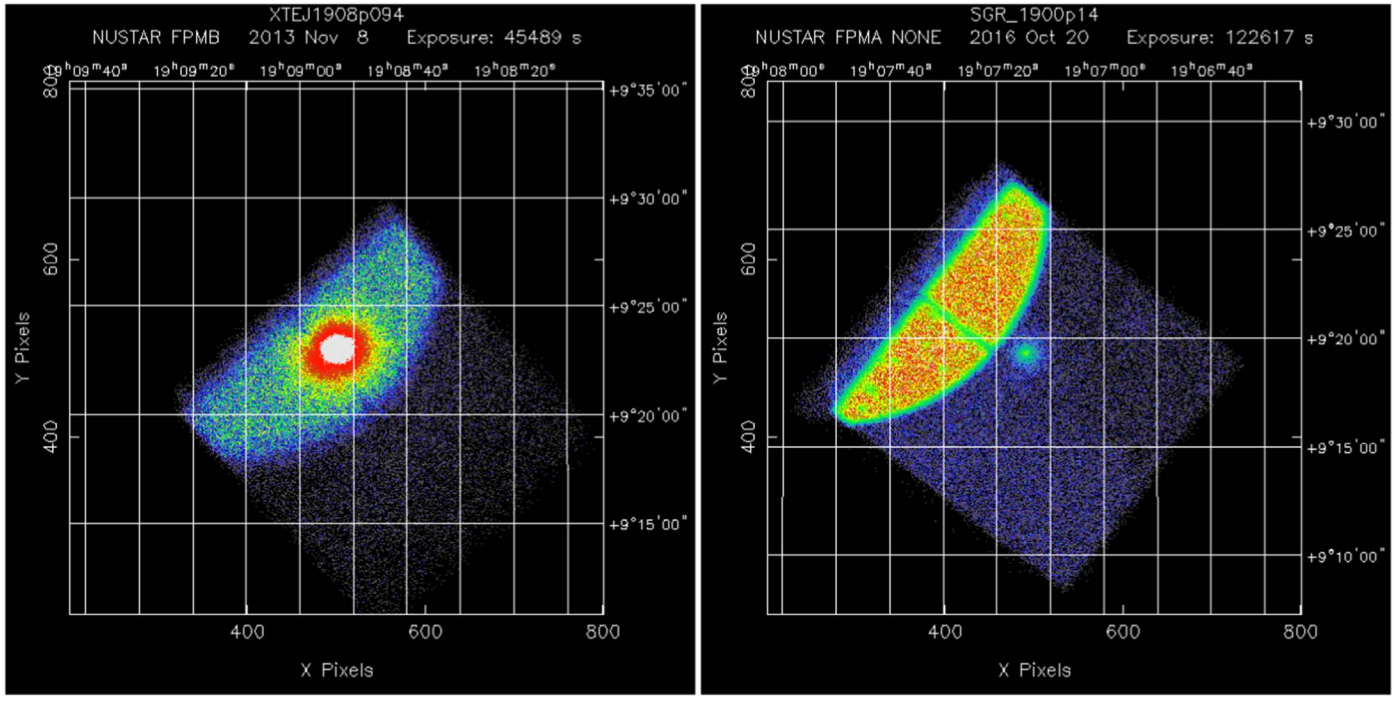

Figure 2. The 3–79 keV NuSTAR quick-look images in "sky" coordinates from HEASARC showing the stray light from GRS 1915+105 along with the X-rays from the targeted source for two epochs (the intended source target name is given in the figure titles). Unlike the point source, which is contained on one detector, the stray light spans multiple detectors on the NuSTAR focal plane.

more straightforward as well. This comes at the reduced effective area for stray light observations compared with pointed observations.

Recently, observations intentionally placing a target so that it is observed via stray light have been undertaken for a number of bright X-ray binaries. This was done to provide contiguous observations while reducing the count rate (and thus the telemetry load) and to potentially extend the spectral range covered by NuSTAR beyond the 78.4 keV cutoff in the optics response. One example is the observation of the Crab Nebula

seen via stray light, which allows for a simple, unique measurement of the spectral shape and flux of the Crab (Madsen et al. 2017b).

In this paper, we describe the NuSTAR StrayCats,[13] a catalog of NuSTAR stray light observations (both serendipitous and intentional) throughout the mission. In Section 2, we describe the preliminary data processing and the stray light identification methodology. In Section 3, we discuss the particular response files needed for StrayCats spectroscopic analysis, as well as the tools that we have developed for streamlining the extraction of StrayCats high-level science products, such as spectra and light curves. In Section 4, we give an overview of the catalog itself, including source lists and demographics, and in Section 5, we present preliminary analyses of several StrayCats data sets to give a demonstration of the type and quality of the data. However, we generally will reserve a more detailed follow-up analysis of individual sources for future work.

2. Data Processing and Stray Light Identification

Identifying observations contaminated by stray light is nontrivial due to the variability in the NuSTAR background contributions, the presence of multiple sources in the FoV, and the different amounts of detector area illuminated by the stray light sources at different off-axis angles. We utilized two complementary methods: an a priori approach based on the location of known bright X-ray sources detected by Swift-BAT and INTEGRAL and a "bottom-up" approach using a statistical approach to identify potential stray light candidate observations.

2.1. An a Priori Approach

We use the Swift-BAT 105 month all-sky catalog (Oh et al. 2018) of sources along with the INTEGRAL 9 yr Galactic plane ($|b| < 17.^{\circ}5$) catalog (Krivonos et al. 2012). These catalogs are both used by the NuSTAR Science Operations Center (SOC) to identify and mitigate sources of stray light contamination for science observations. To estimate the amount of stray light in a given observation, we utilize the nustar_stray_light IDL code.[14] This contains a model of the size, shape, and relative positions of the focal plane structures (seen in Figure 1) and the bench that holds the NuSTAR optics. For a given NuSTAR pointing orientation and stray light target, the "shadow" from the aperture stop and optics bench is projected onto the focal plane for each detector to estimate the stray light contribution.

Estimating the strength of the stray light is done by extrapolating the measured spectrum in the Swift-BAT/INTEGRAL bands down into the NuSTAR stray light bandpass (3–20 keV), a process that frequently results in overestimating the NuSTAR flux for sources that have curvature in the hard X-ray bandpass or a predominantly thermal spectrum. Nonetheless, there is usually a reasonable match between the brightest catalog sources and the stray light in NuSTAR.

As a first step, we produce an estimate catalog of all NuSTAR observations within 4° of a "bright" X-ray source in one of our reference catalogs, where we typically define the minimum flux level for a persistent, bright source to be >5 mCrab, as measured by the respective instruments on INTEGRAL and Swift. This results in several hundred NuSTAR stray light candidate observations. For each observation, we produce the estimated stray light map and visually compare the results to the observed data. As many of these sources are variable and the internal model of the structures may not be entirely accurate, this does require a human in the loop for positive identification of a stray light candidate. While this process is able to positively identify dozens of stray light observations, it is inefficient and does not catch any stray light observations of new or intermittently transient sources.

2.2. A More Statistical Approach

Rather than requiring any prior knowledge of a nearby bright target, we instead use the observed data to identify stray light candidates. Since the area of the sky accessible to each NuSTAR telescope for stray light is different, we treat the two separately.

We first remove contributions from the primary target by first excising all counts from within 3′ of the estimated target location. This large exclusion region attempts to account for any astrometric errors between the estimated J2000 coordinates for the target and where the target is actually observed to reduce the "PSF bleed" from bright primary targets. For bright primary targets (those with focused count rates >100 cps), we find that the primary source dominates over the entire FoV, so we exclude these observations from consideration. Once this is complete, we compute the 3–20 keV count rate for all four detectors on each focal plane module (FPM) and combine them to account for the fact that the stray light patterns tend to illuminate one side (or all) of the FoV.

For the remaining sources, we flag observations where the count rate measured by a particular detector combination deviates from the mean. Unfortunately, due to extended sources, fields with multiple point sources, and intrinsic variation in the NuSTAR background, all of the candidate StrayCats observations had to be further checked by eye. We do this by constructing DET1 images in the 3–20 keV bandpass and looking for the signatures of stray light. Figure 3 shows a selection of StrayCats observations where the stray light can clearly be seen.

We continue the iterative process to identify the candidates described above until all of the candidates appear to be simply variations in the NuSTAR background and not clearly associated with stray light. Overall, more than 1400 candidate stray light observations were checked by hand for the presence of stray light.

We feel confident that we have thus identified all of the stray light sources that could (a) produce a strong enough signal to impact the science analysis of the primary target and (b) be useful for scientific analysis in their own right. These fully vetted StrayCats sources form the basis for the full catalog. In addition to stray light, we have also identified a number of observations where targets just outside of the NuSTAR FoV result in "ghost rays," where photons perform a single bounce off of the NuSTAR optics rather than the double bounce for focused emission (Madsen et al. 2017a). These are included in StrayCats for completeness.

We note that this human-in-the-loop approach results in a bias where faint stray light sources are more easily seen during long exposures. Similarly, sources with transient flaring

[13] https://nustarstraycats.github.io/
[14] https://github.com/NuSTAR/nustar-gen-utils

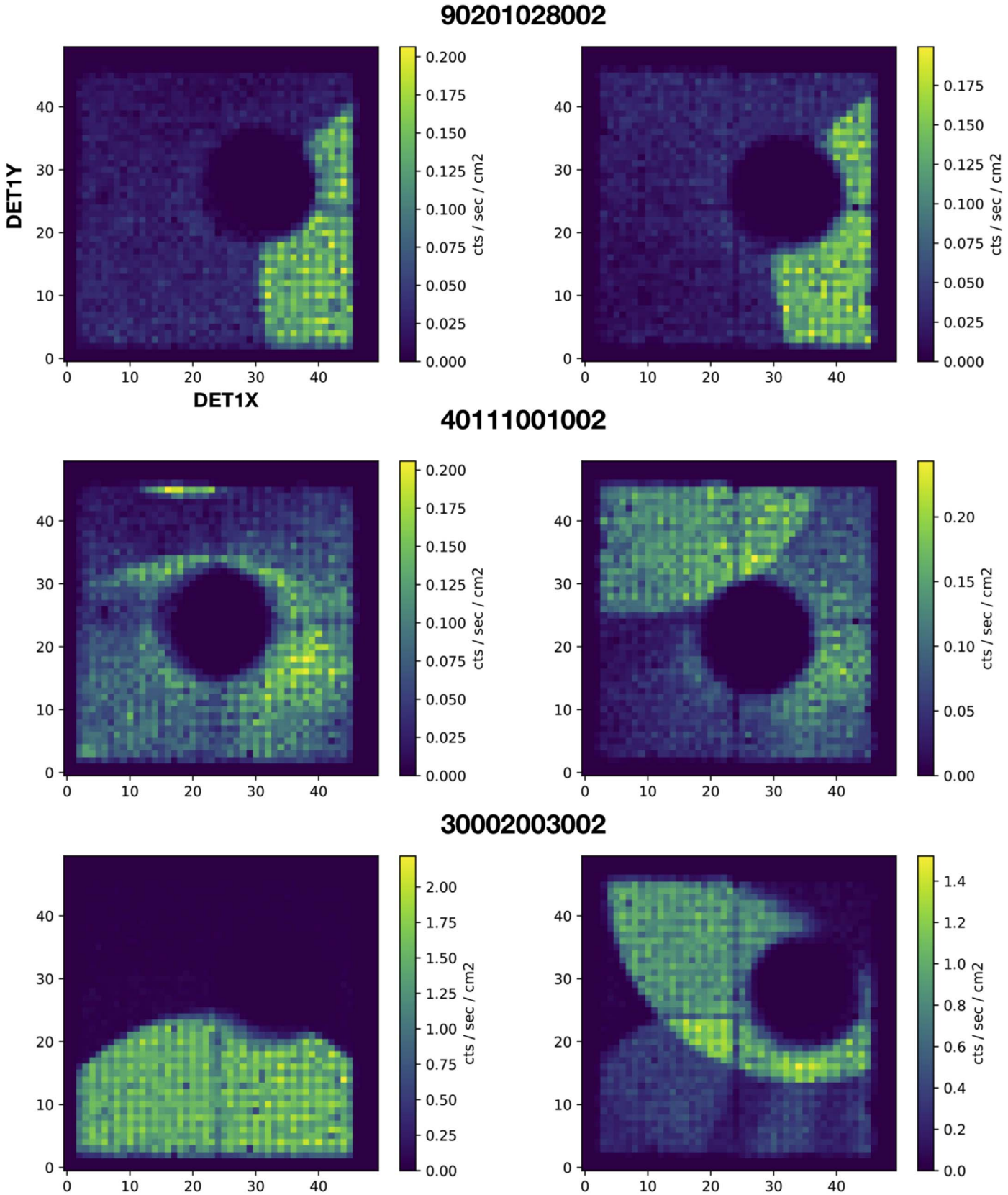

Figure 3. Rogue's gallery of 3–20 keV NuSTAR images in DET1 pixel coordinates (1 pixel = $2\farcs54 = 120.96\ \mu$m) for three `StrayCats` observations showing some of the variety of the stray light patterns in FPMA (left column) and FPMB (right columns). The primary source has been masked out, and the linear color scale shows the fluence (counts per second per square centimeter) across the FoV for each detector. (Top) One of the cases where stray light (here from the LMXB 4U 1624–490) is seen in both FPMs. (Middle) A more complex geometry where multiple overlapping or partially blocked stray light sources (the strongest being 4U 1708-40 in FPMA and 4U 1700–377 in FPMB) overlay the extended primary source (RX J1713.7–3946). (Bottom) Strong and overlapping stray light from GX 5–1 (lower SL) and GX 3+1 (upper right in FPMB).

behavior on timescales of a few hundred seconds will be difficult to identify unless the quiescent flux level is greater than that of the standard NuSTAR background. We anticipate that a further investigation for transients could produce a number of additional StrayCats candidates, though this is beyond the scope of this first work.

3. The StrayCats Catalog

The StrayCats Catalog is intended to be used by observers looking for serendipitous observations of bright galactic (including the LMC and SMC) sources beyond what is available through traditional monitoring observations. The catalog is available via a simple web interface[15] or through a FITS file that identifies which NuSTAR sequence IDs contain StrayCats sources. For observations that contain multiple StrayCats sources, the web interface also contains diagnostic information that can be used to determine which stray light pattern is associated with a particular source (i.e., the images shown in Figure 3). An excerpt of the table is given in the Appendix in Table 4.

The first version of StrayCats includes the following columns.

1. StrayID. The StrayCats catalog identifier, which is StrayCatsI_XX, where XX is the row number after the catalog is sorted by the R.A. and decl. for the NuSTAR sequence ID.
2. Classification.
   (a) SL. The source has been positively identified as a StrayCats target.
   (b) Complex. Stray light is present, but there are multiple overlapping stray light regions that make the sources difficult to identify.
   (c) Faint. Stray light is present but too faint to be positively identified.
   (d) GR. The observation contains ghost rays from sources just outside of the FoV.
   (e) Unkn. A stray light pattern is present, but the source of the stray light remains unknown.
3. SEQID. The NuSTAR sequence ID.
4. Module. The NuSTAR FPM that contains the stray light (A or B).
5. Exposure. The exposure time for this observation in seconds.
6. Multi. Whether the sequence ID contains multiple stray light patterns (Y or N).
7. Primary. The name of the primary target for the pointed science observation.
8. TIME/END_TIME. The MJD start/end of the observation.
9. RA/DEC_Primary. The R.A./decl. of the primary target.
10. SL source. The name of the source of stray light if we have identified it.
11. SL type.

For sources with a positive identification, we have made an effort to sample the literature and provide a source classification. Many of these are relatively famous sources identified by GINGA or Uhuru with a large literature background, so we do not provide prime references for the classifications in StrayCats. For sources with a classification other than SL, this defaults to "??." Classification types are as follows.

1. AGN (active galaxy).
2. LMXB (low-mass X-ray binary) with -NS or -BH if the compact object type is known.
3. HMXB (high-mass X-ray binary) with -NS or -BH if the compact object type is known.
4. Pulsar/PWN (pulsar wind nebula)/NS.
5. BHC (BH candidate).
6. SNR (supernova remnant).
7. Cluster (galaxy cluster).
8. Radio galaxy.

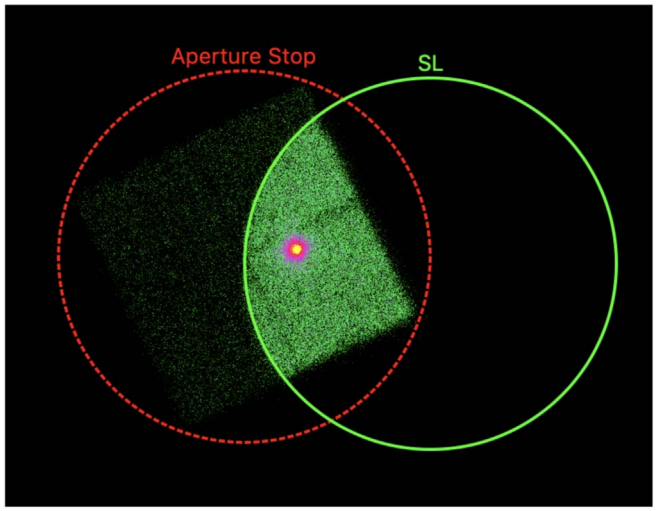

Figure 4. Example of the stray light (green) and aperture stop (red) regions that can be used to identify the source location on the sky. See text for details.

1. SIMBAD_ID. The identifier that can be used via SIMBAD to identify the source. This can often be different than the source name in the all-sky catalogs used to identify the source (if known, otherwise defaults to NA).
2. RA/DEC_SL. The R.A./decl. of the source of the stray light (if known, otherwise defaults to −999).

StrayCats contains 436 telescope fields (with A and B counted separately) containing stray light from 78 confirmed StrayCats sources. During the visual inspection of the stray light candidates, we compare the observed stray light patterns with those predicted for that observation using the same code used in Section 2.1. For a majority of sources, this is sufficient to identify the source of stray light. For a few dozen cases, the stray light is associated with a source that is not present in either catalog. This is because the source is either a new transient (e.g., a number of MAXI-identified transients that went into outburst over the last few years), only occasionally detected by the all-sky hard X-ray detectors (e.g., sources contained in the "Swift-BAT historically detected" list), or typically too soft to be detected by Swift-BAT or INTEGRAL. We have not yet identified any previously unknown StrayCats sources.

We can estimate the source location using the projected shape of the aperture stop on the focal plane. Figure 4 gives an example of this for a simple case. Here the curvature of the

[15] https://nustarstraycats.github.io/

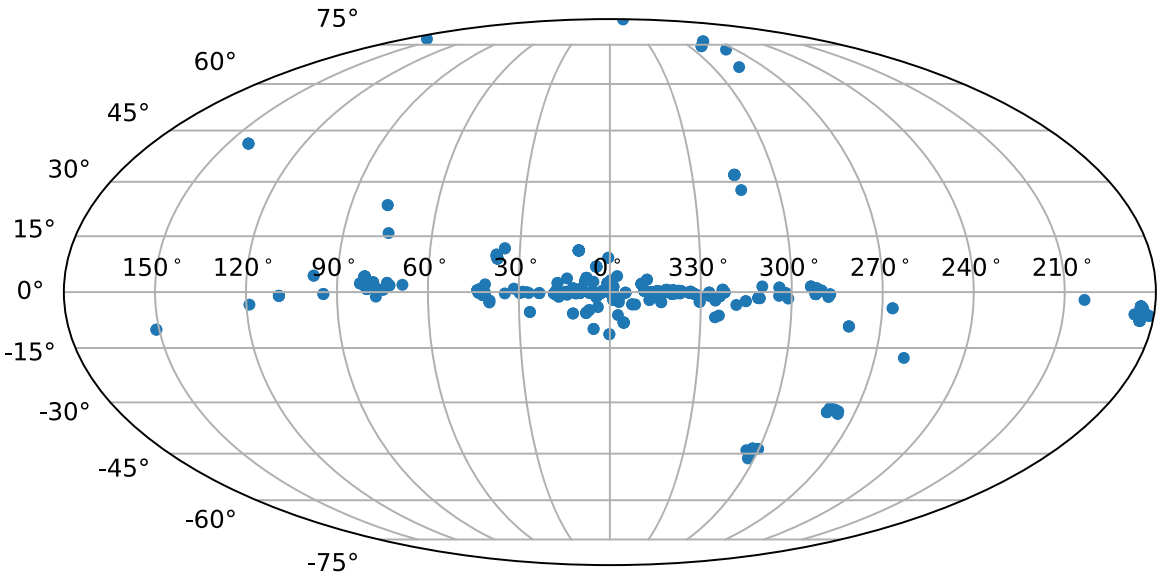

Figure 5. Distribution of StrayCats in galactic coordinates showing the clustering of these sources near the Galactic plane, the contribution from bright sources in the LMC and SMC, and a few AGN located out of the plane of the Galaxy. The coordinates shown here are for the primary (focused target).

aperture stop shadow is clearly seen on the focal plane. We generate an "SL" region that matches the known curve and compute the offset between this and the center of the FoV (the "aperture stop" region in Figure 4). We can compute the offset on the focal plane (in millimeters) and leverage the fact that we know that the deployed aperture stop is 833.2 mm (F. Harrison 2021, private communication) away from the focal plane to convert this offset to an angular offset. The direction of the shift (in sky coordinates) allows us to determine the position angle of the shift. In the example shown here, we were able to reproduce the location of Cir X-1 to better than 10′, which is generally good enough to identify the source. For cases where multiple overlapping stray light patterns are seen and we cannot unambiguously identify the source, we assign the "Complex" classification pending a detailed analysis.

The catalog contains seven AGN and one galaxy cluster, several pulsar wind nebulae and supernova remnants, roughly 17 accreting BHs (including BH candidates), and over 40 accreting NSs, including several pulsars and a number of known type I X-ray bursters. Figure 5 shows the Galactic distribution of these sources, where the density of sources near the Galactic plane and the LMC and SMC can clearly be seen.

4. StrayCats Data Analysis Tools and Response Files

The StrayCats data requires subtly different analysis methods than those typically used for focused NuSTAR observations. Rather than working in "SKY" coordinates like focused observations, for stray light observations, we instead work in "detector" coordinates (DET1 coordinates in NuSTAR vernacular). This coordinate system is fixed with respect to the NuSTAR CdZnTe detectors, and, in these coordinates, the pattern of stray light on the focal plane is predominantly sensitive to the observatory orientation and extremely weakly coupled to any motion of the NuSTAR mast. For pointed observations, the ∼millimeter-scale motion of the NuSTAR mast affects the throughput of the optics by changing the distance of the source from the optical axis ("vignetting"; Harrison et al. 2013). In nonfocused observations, the mast motion only minimally changes the shadow pattern as observed by the detectors and can be neglected.

Producing high-level science products for a StrayCats observation is relatively straightforward. These mostly deal with properly tracking the production of "source" region files and applying spatial filtering on the NuSTAR data in DET1 coordinates. Our goal is to make the resulting products as similar to standard NuSTAR products as possible for ease of use.

To date, we have contributed a number of high-level "wrappers" to the NuSTAR community-contributed GitHub page.[16] These are largely written in python and significantly leverage the existing astropy framework (Robitaille et al. 2013; Astropy Collaboration et al. 2018), as well as the multimission FTOOLs distributed by HEASARC, such as XSELECT. Final high-level products are mostly generated using NUPRODUCTS from the NUSTARDAS software with a number of nonstandard configuration settings. This allows a user to easily produce standard spectrum (PHA) and light-curve files, as well as response matrix functions that can be directly loaded into downstream analysis software, such as XSPEC (Arnaud 1996) or ISIS (Houck & Denicola 2000) for spectral analysis or STINGRAY (Huppenkothen et al. 2019) for timing analysis.

4.1. Response Files

The one unique requirement for the analysis of StrayCats observations is the production of the response files. For a focused observation, each count is first "projected" onto the sky, and the optics response (i.e., the ancillary response file, or ARF) is produced so that it accounts for the time-dependent drift in the location of the optical axis due to the thermal motion of the NuSTAR mast. The ARF is generated starting with an on-axis optics response, which is then convolved with an energy-dependent vignetting function based on the off-axis angles sampled by the source. Finally, the ARF also includes the attenuation along the photon path due to the optics thermal

[16] https://github.com/NuSTAR/nustar-gen-utils

covers, the Be window protecting the detectors, and the absorption features in the CdZnTe detectors themselves.[17]

Since for StrayCats observations, we are working in DET1 coordinates, we no longer need to account for the time-dependent variations in the ARF or (obviously) the response of the optics themselves. The StrayCats ARF instead only needs to account for the amount of illuminated area on the focal plane (for overall normalization, given in square centimeters) and any energy-dependent absorption due to the Be window and losses in the CdZnTe detectors. All of these contributions are currently stored in the NuSTAR CALDB files (with the exception of the Be window attenuation, which is subsumed into the on-axis ARF in the CALDB). The ARF generation tool for StrayCats analysis properly reads these files from the NuSTAR CALDB and weights the response based on the illuminated area on each focal plane detector. The resulting file can be directly imported into XSPEC along with the other spectral files above for analysis. This approach has been validated against observations of the Crab (Madsen et al. 2017b).

Absorbed stray light (stray light that partially penetrates through the aperture stops; see Madsen et al. 2017a) is not accounted for here. These response files only account for the unabsorbed stray light that reaches the focal plane. In addition, two of the sources in StrayCats are extended sources (Cas A and the Coma Cluster). Analyzing data from extended sources is more complex and beyond the scope of this analysis. Analyzing these sources in detail will likely require bespoke ray-trace simulations to properly interpret the stray light spectrum.

4.2. Region Files

While all of the StrayCats clearly show the effects of stray light, the scientific usefulness of the observations will depend on how much of the FoV is covered by stray light. In the case of the intentional stray light observations mentioned above, the NuSTAR observations were designed to maximize the amount of detector area illuminated by stray light, which results in roughly half of the 16 cm^2 detector area being illuminated (compared with the on-axis effective area of $\approx$400 cm^2 for each NuSTAR telescope). For standard observations, the NuSTAR SOC attempts to minimize this coverage when possible, so the illuminated detector area for the serendipitous StrayCats observations varies dramatically. Because the stray light pattern depends on the shadowing of the detectors by the optical bench, NuSTAR is also rarely in an orientation where stray light is present on both NuSTAR FPMs.

Due to the large number of StrayCats observations and the geometrically complex region shapes, we developed a semiautomated approach to reducing the amount of manual effort involved in generating the optimal extraction region. The wrapper for this approach is available on the aforementioned NuSTAR GitHub page. For StrayCats containing a bright point source, the first step of this process is point-source removal. This is done by first determining the position of the targeted source in DET1 coordinates (using the nuskytodet FTOOL). This location depends on the motion of the NuSTAR mast and any changes in the NuSTAR pointing, so we determine the radial distance from each observation count from this position. We screen events within r arcminutes of the source (if necessary, and where the choice of r is chosen on a case-by-case basis) and generate an image in an adjustable energy band (the 3–10 keV band is the default).

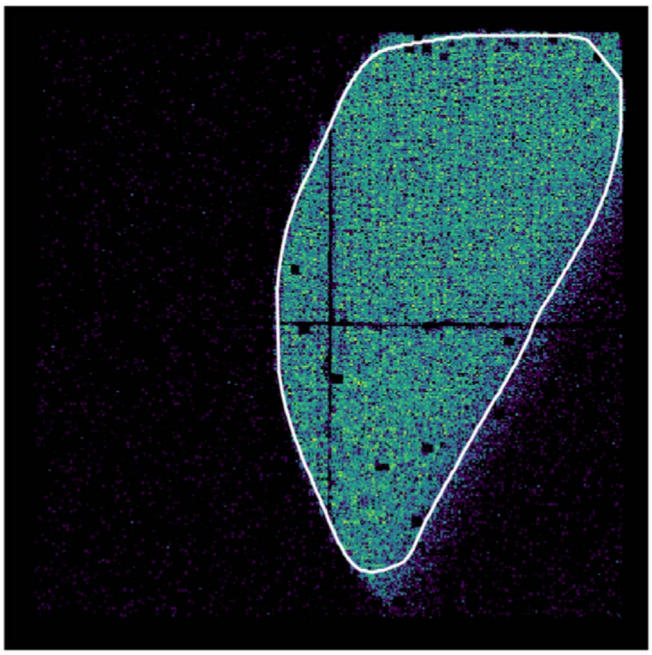

Figure 6. Example of a semiautomatically generated region for a StrayCats observation of the Crab.

We use Canny edge detection from scikit-image[18] to generate the polygons used to estimate the source region, where the width of the Gaussian filter used by the Canny edge detection (σ) is an adjustable parameter. Again, this is chosen on a case-by-case basis such that the filter accurately identifies the edges of the stray light region. Polygon region corners in image coordinates are determined from the detected edge pixels and used to write a region file in SAOImageDS9 standard format using the regions astropy-affiliated module.

This approach is particularly useful for stray light regions with an angular cutaway resulting from the shadow of the optical bench (i.e., Figure 6). This process is most efficient for intentional stray light observations and serendipitous observations containing a single stray light pattern from only the "SL target" source (i.e., entries in the StrayCats catalog with the classification "SL" and multi value "N"). Currently, this approach is most limited by the σ parameter, which approximately ranges between 3 and 12 for optimal stray light observations but can vary greatly for weak stray light regions. Discontinuities in the edges identified by the Canny filter occasionally result in the created polygon region omitting (sometimes negligibly thin) slices of the stray light region; these anomalies can often be corrected by fine-tuning σ. However, there are no optimal σ values for the Canny filter to properly identify the stray light region for observations in which the fluxes of the background and the stray light are comparable. Future improvements to this process that eliminate the manual determination of the point-source removal limit and Canny edge detector σ would allow for fully automated region extraction.

[17] See the NuSTAR software user's guide: https://heasarc.gsfc.nasa.gov/docs/nustar/analysis/nustar_swguide.pdf.

[18] https://scikit-image.org

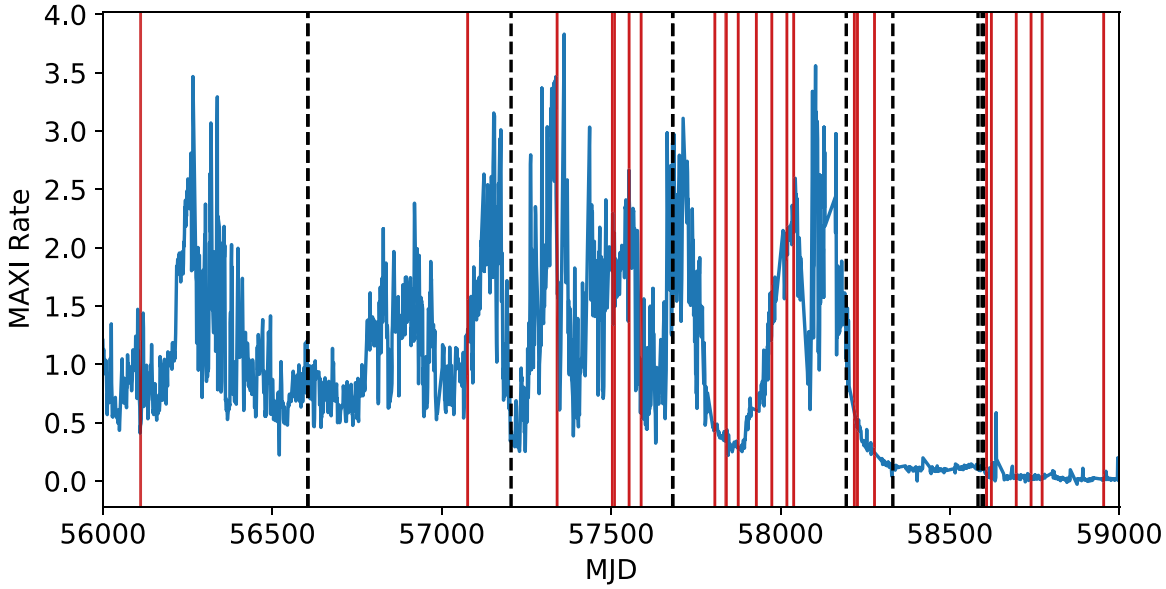

Figure 7. Long-term 2–10 keV light curve of GRS 1915+105 as measured by MAXI (blue line), along with the timing of the focused NuSTAR observations (red lines) and the `StrayCats` observations (dashed black lines). The final three epochs are clustered in the 16 days just before MJD 58,600.

4.3. Background

Dealing with background for `StrayCats` sources is not trivial. For standard NuSTAR pointed obervations, standard techniques such as using a neighboring source-free region to estimate the background and/or estimating the NuSTAR background through tools such as `nuskybgd` (Wik et al. 2014) can be used "out of the box." However, as we are using NuSTAR as a collimator rather than a focusing telescope, the background must be treated with more care.

The `StrayCats` source regions cover a large region of the FoV (and there may be multiple `StrayCats` sources, as well as the primary source in the FoV), so selecting a background region may be difficult. In addition, for bright `StrayCats` sources, some stray light may also be transmitted through the aperture stop at higher energies, making it impractical to select a neighboring "source-free" region of the FoV to use to estimate the background (see Madsen et al. 2017a, 2017b, for further discussion).

Modeling the background contributions must also be handled with care. Because many of the `StrayCats` sources are near the Galactic plane, the standard models of the spatial variation of the NuSTAR background used by `nuskybgd` to model the contributions from the Galactic ridge X-ray emission (GRXE; Krivonos et al. 2007) are largely untested and may need to be adapted for the nonisotropic shape of the GRXE.

The exact method used to handle the presence of background will necessarily vary depending on the science goals for the individual analysis. For bright, hard sources, even without the aid of the NuSTAR optics, the backgrounds in NuSTAR are so low that the background may be neglected up to high energies. For fainter sources (or soft sources), the energy at which the background starts to significantly contribute (and therefore the background component that matters the most for spectral analysis) will depend on the details of the source flux. We do not expect there to be a universal solution or recommendation for how to handle the backgrounds.

In the selected preliminary results below, spectral analysis is typically halted when the source flux falls so that the background is estimated to be ∼10% of the source flux, but we stress that a thorough treatment of the background must be considered.

5. Selected Preliminary `StrayCats` Results

5.1. GRS 1915+105

The LMXB system GRS 1915+105 has been in outburst since its discovery in 1992 (Castro-Tirado et al. 1992) and shows a wide range of source spectral and timing states (e.g., Belloni et al. 2000). The system is known to host a near-maximally spinning BH (McClintock et al. 2006), and observations of the absorption features also reveal the presence of a complex outflowing disk wind (Miller et al. 2016). However, the source began a decay to either a quiescent or a highly absorbed state between 2018 and 2020 (Miller et al. 2020; Neilsen et al. 2020). Since 2012, NuSTAR has observed the source a number of times at varying flux levels (Figure 7). However, the high count rates from this source present two key problems that affect the scientific return from these data. (1) NuSTAR has a fixed 2.5 ms dead time per event, resulting in a maximum throughput of 400 counts s^{-1}. In high-rate sources, this dead time also results in the effective exposure being much lower than the time spent observing the target. (2) As mentioned above, the high count rates result in high telemetry loads that require short-duration observations to avoid data loss on board. GRS 1915+105 also appears in six `StrayCats` epochs, covering a wide range of flux states (Figure 10) as measured by the Monitor of All-sky X-ray Image (MAXI) instrument on the International Space Station (Matsuoka et al. 2009). The durations of the `StrayCats` observations vary, from several snapshots of roughly 20 ks effective exposure to several deep observations with over 120 ks of exposure. A summary of the `StrayCats` for GRS 1915+105 is given in Table 1.

As an example, we show preliminary results from one epoch (Obs. 3A, 30201013002; Figure 8), which had an effective exposure of 122 ks spanning roughly 240 ks (over 2.5 days) of

Table 1
GRS 1915+105 StrayCats Observations

Obs. No.	Sequence ID	Obs. Date	MJD	FPM	Exp. (ks)	Area (cm^2)
1A	80001014002	2013-11-8T18:11:07	56,604.8	A	45.15	3.9
1B	…	…	…	B	45.49	4.0
2	30101050002	2015-07-1T15:31:08	57,204.6	A	41.34	[a]
3A[b]	30201013002	2016-10-20T16:56:08	57,681.7	A	122.3	2.2
3B	…	…	…	B	122.6	3.6
4	40301001002	2018-03-17T01:46:09	58,194.1	A	125.6	5.9
5	30401018002	2018-08-1T12:41:09	58,331.5	B	78.3	4.9
6	90501317002	2019-04-10T01:26:09	58,583.1	A	40.8	5.7
7	30402026002	2019-04-22T00:11:09	58,595.0	A	18.83	[a]
8	30402026004	2019-04-26T13:41:09	58,599.6	A	23.31	[a]

Notes.
[a] Small stray light area.
[b] Used for the analysis in this work.

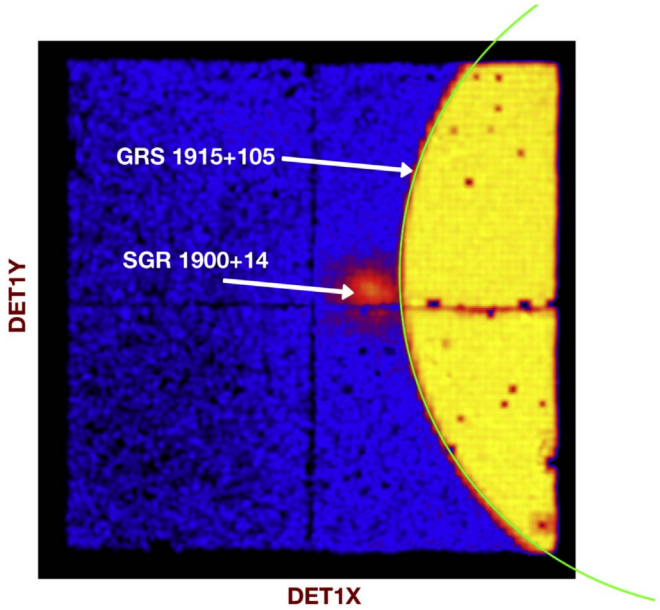

Figure 8. The 3–20 keV DET1 image for sequence ID 30201013002. The faint primary source is shown, as is the stray light pattern for GRS 1915+105 along with the region showing the shadow of the aperture stop.

clock time. The epoch-averaged source spectrum (Figure 9) shows that the source is clearly detected up to at least 40 keV before the background becomes a significant contribution to the spectrum. At low energies, we clearly see evidence for Fe-line and absorption features typically associated with disk winds in this system (e.g., Miller et al. 2016; Neilsen et al. 2018).

However, the spectrum for this source is known to be highly variable, with the source hardness varying with the apparent emission states, and throughout this extended observation, the source showed a variety of emission states. For example, during the first orbit, we clearly observe quasiperiodic oscillations (QPOs) in the form of 10–20 s recurrent "pulsations" of emission, while in later orbits during the same observation, the source has transitioned to its θ state, showing emission building up over the span of a few hundred seconds before sharply dropping away (Figure 10). A detailed analysis of the spectral changes throughout this system is beyond the scope of this work (e.g., Zoghbi et al. 2016) but shows the

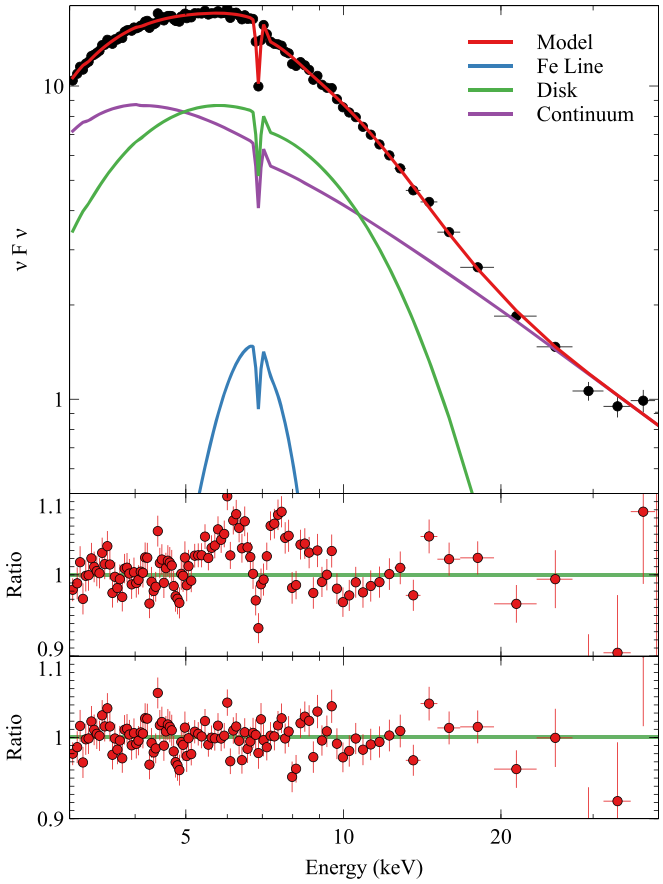

Figure 9. Integrated spectrum from Obs. 3A from a portion of the stray light region. A similar-sized region was used to estimate the background. The base model spectrum here consists of a hot accretion disk component and a soft nonthermal power law, though this leaves strong residuals near the Fe line (middle). We find that after the addition of a broad Fe line and absorption features associated with disk winds in this system that we obtain a reasonable fit to the data.

utility of only one of the several observations of GRS 1915+105.

5.2. GX 3+1

GX 3+1 is a persistently accreting "atoll" source. Atoll sources trace out regions on hardness–intensity diagrams that

Table 2
GX 3+1 StrayCats Observations

Obs. No.	Sequence ID	Obs. Date	FPM	Exp. (ks)	Area (cm^2)
1	30002003003	2013-06-19T09:31:07	B	∼29	3.51
2	80002017002	2014-02-15T05:36:07	A	∼39	4.64
3	90101012002	2015-08-11T22:51:08	B	∼49	1.46
4	90101022002	2016-02-18T22:26:08	A	∼36.7	3.79
5	40112003002	2016-03-17T00:31:08	A	∼52	1.35
6	80102101002	2016-09-29T21:21:08	B	∼29.5	6.33
7	80102101004	2016-10-19T15:01:08	B	∼28	7.15
8	80102101005	2016-10-31T20:11:08	B	∼29	6.66
9	80202027002	2017-02-18T14:31:09	A	∼31	4.69
10[a]	40112002002	2017-04-03T18:31:09	A	∼100.7	4.18
11	90402313004	2018-04-14T02:56:09	A	∼61	3.40
	…	…	B	∼61	3.43
12	90501329001	2019-06-22T07:51:09	B	∼40	3.35
13	90501343002	2019-10-1T22:36:09	B	∼37	1.65
14	90601317002	2020-05-7T07:06:09	A	∼49	4.12

Note.
[a] Used for the analysis in this work.

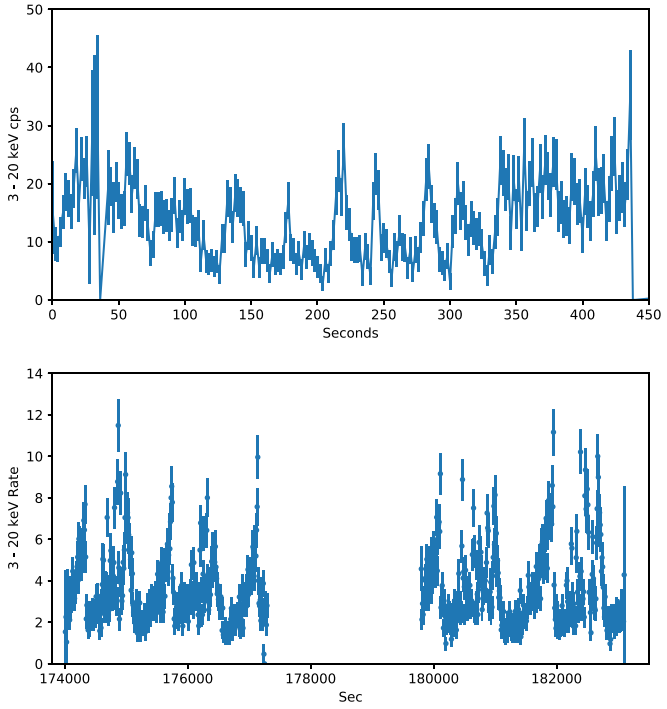

Figure 10. The 3–20 keV light curve for the first 450 s of the first orbit binned at 2 s resolution shows the presence of transient slow (mHz) QPO signals. (Bottom) The 3–20 keV light curve of two later orbits binned at 10 s resolution showing that the source has transitioned to its θ state.

resemble "islands" (for which they are named; Hasinger & van der Klis 1989) or "banana" shapes. GX 3+1 exclusively occupies the banana branch (Seifina & Titarchuk 2012) and was serendipitously observed via stray light in NuSTAR 19 times between 2012 July and 2020 May. Table 2 shows the sequence ID, observation date, FPM that the stray light occurred on, exposure time, and area on the FPM for observations with an area greater than 1 cm^2 of stray light from the source. Light curves were generated in three different energy bands (3–20, 6.4–10, and 10–16 keV) with a bin size of 300 s. Figure 11 shows the hardness–intensity diagram for GX 3+1. The hardness ratio (HR) is defined as the 10–16 keV band divided by the 6.4–10 keV band (Coughenour et al. 2018). The source traces out the banana branch.

To demonstrate the spectral utility of stray light observations for studying NS LMXBs, we extract a spectrum from the longest observation, Obs. 10. The data are fit with the three-component model of Lin et al. (2007) that was used in Ludlam et al. (2019) for the pointed observation of GX 3+1. This is comprised of a multitemperature blackbody for thermal emission from the accretion disk, single-temperature blackbody for a boundary layer or emission from the NS surface, and power law for weak Comptonized emission. For direct comparison to the intentional NuSTAR observation, we model the continuum emission by fixing the absorption column along the line of sight, blackbody temperatures, and photon index to the values reported in Table 2 of Ludlam et al. (2019) while allowing for the normalizations of each spectral component to vary. The spectrum and continuum components are shown in Figure 12. The color scheme and line types correspond to those in Ludlam et al. (2019). Indeed, a prominent Fe line emission feature can be seen in the stray light observations akin to the one observed from the pointed observations (see Figure 1 of Ludlam et al. 2019). Further details of the variations in this source over time will be addressed in future work.

5.3. GS 1826–24

GS 1826–24 is an LMXB that showed remarkably consistent type I X-ray bursts since its discovery by GINGA (e.g., Ubertini et al. 1999). The type I X-ray bursts were so regular as to earn this source the "clocked burster" moniker. A sudden dip in the Swift-BAT 15–50 keV light curve resulted in a NuSTAR ToO observation of this source in 2014 (Chenevez et al. 2016). After briefly returning to a hard state, the source appears to have transitioned into a "soft" state in 2016 with the MAXI light curve increasing to a plateau in 2018 and the Swift-BAT light curve in an apparently quiescent state (Figure 13). While there have not been any subsequent targeted observations with either NuSTAR or

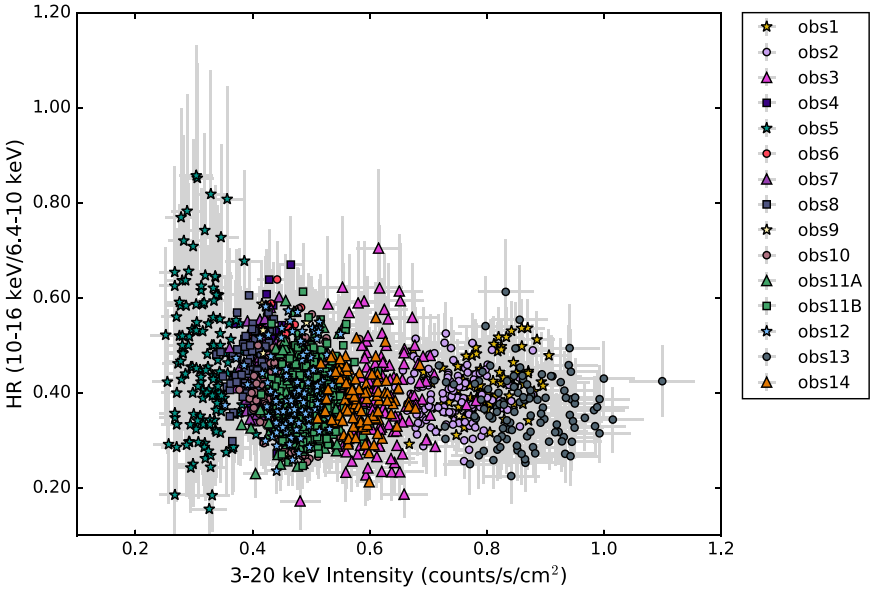

Figure 11. Hardness–intensity diagram of the stray light observations of GX 3+1. Observation numbers refer to the sequence IDs in Table 2. Data are binned to 300 s. The banana branch is traced out by the data.

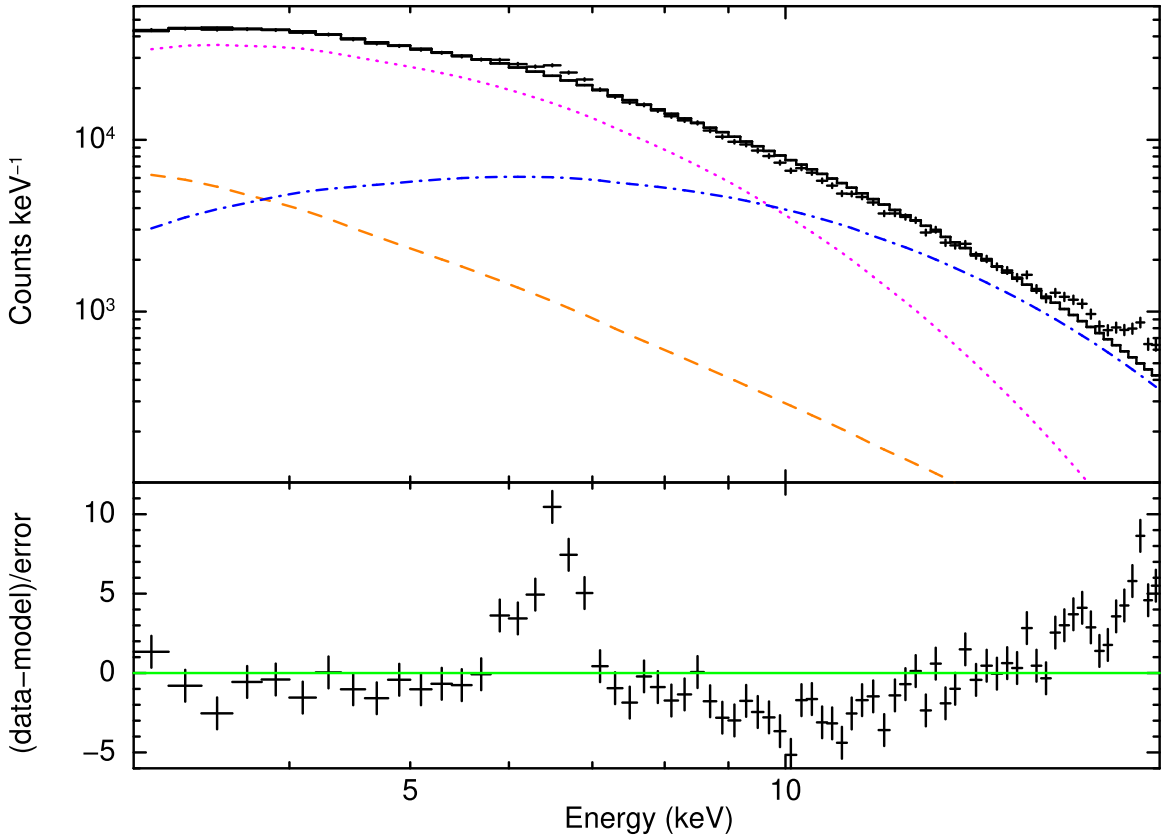

Figure 12. The 3–20 keV stray light spectrum of GX 3+1 Obs. 10 and residuals divided by the error. The orange dashed line indicates the power-law component, the blue dotted–dashed line is the single-temperature blackbody, and the magenta dotted line is the multitemperature blackbody. A prominent Fe line feature is present between 6 and 7 keV. The background begins to dominate above 15 keV.

XMM, NICER has monitored the source and found evidence for mHz QPOs (Strohmayer et al. 2018).

The `StrayCats` observations (Table 3) span both the predip observations and include several long observations during the BAT X-ray minimum. We highlight one of these (Obs. 7), which had a substantial amount of stray light covering over half of FPMB and a long exposure of over 150 ks, resulting in nearly 300 ks of elapsed clock time. During this observation, NuSTAR clearly detected two type I X-ray bursts lasting ∼10 s (Figure 14). Simultaneously, the X-ray flux in the 3–20 keV light curve dipped leading up to the burst itself. We only find two type I X-ray bursts, while we would have

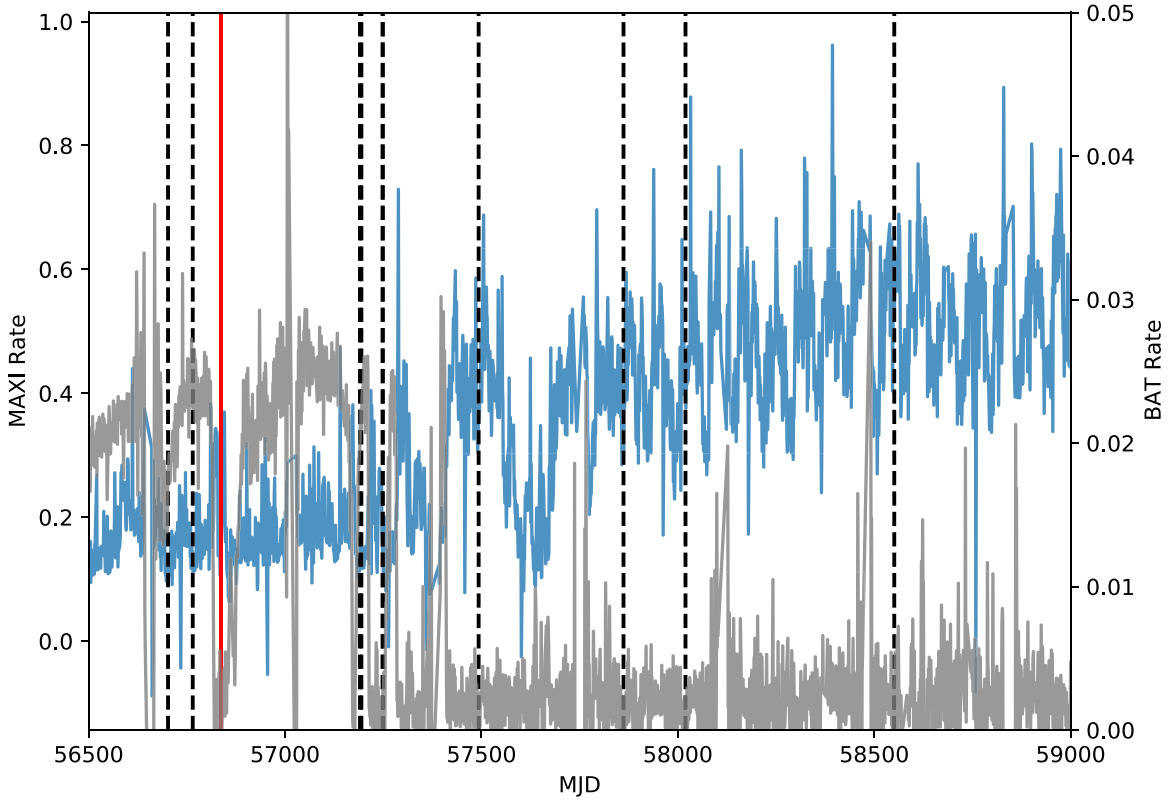

Figure 13. Long-term 2–20 keV MAXI light curve (blue) and Swift-BAT transient monitor 15–50 keV light curve for GS 1826–24 (gray). The timing of the focused NuSTAR observation is shown by a solid red line, while the timing of the `StrayCats` observations is shown in dashed black lines.

Table 3
GS 1826–24 `StrayCats` Observations

Obs. No.	Sequence ID	Obs. Date	MJD	FPM	Exp. (ks)	Area (cm^2)
1	80002012002	2014-02-14T00:36:07.184	56,702.0	A	24.05	2.2
2	80002012004	2014-04-17T22:46:07.184	56,764.9	A	26.42	2.3
3	30101053002	2015-06-17T16:06:07.184	57,190.7	A	131.32	2.75
4	30101053004	2015-06-21T07:11:07.184	57,194.3	A	51.52	2.5
5	60160692002	2016-04-14T18:26:08.184	57,492.8	B	21.88	1.7
6	10202005002	2017-04-18T13:06:09.184	57,861.5	A	156.51	2.52
7[a]	10202005004	2017-09-23T08:36:09.184	58,019.4	B	156.54	8.8
8	80460628002	2019-03-8T20:21:09.184	58,550.8	B	41.39	1.6

Note.
[a] Used for the analysis in this work.

expected over a dozen had the source been regularly bursting with a recurrence time of ∼5.7 hr (Ubertini et al. 1999). This confirmed the results of the single set of pointed NuSTAR observations that the "clocked" nature of the source has disappeared in the soft state (Chenevez et al. 2016). A more complete survey of the bursting state over all seven epochs and correlations with the spectral changes in the source will be the topic of a future paper.

6. Summary and Future Work

In this paper, we have presented a summary of a unique, untapped set of NuSTAR observations. The `StrayCats` observations found thus far are predominantly associated with known bright sources and transient X-ray binaries as they go into outburst.

`StrayCats` is based on a systematic approach to mining the database of NuSTAR observations. While these observations were previously considered a nuisance, we have now produced a set of publicly available tools for analyzing these data and producing high-level science products. In addition, we provided access to scripts that help in the generation of region files, which often requires some fine-tuning based on the projected "shadow" of the optics bench.

We consider the `StrayCats` catalog that we present here to be version 1.0. We intend to extend the current version of `StrayCats` to include additional summary data products (such as count rates, HRs, and source and background extraction regions) for all `StrayCats` observations where the source is bright enough and enough of the focal plane is covered by stray light. This work is ongoing and will be provided in a future release.

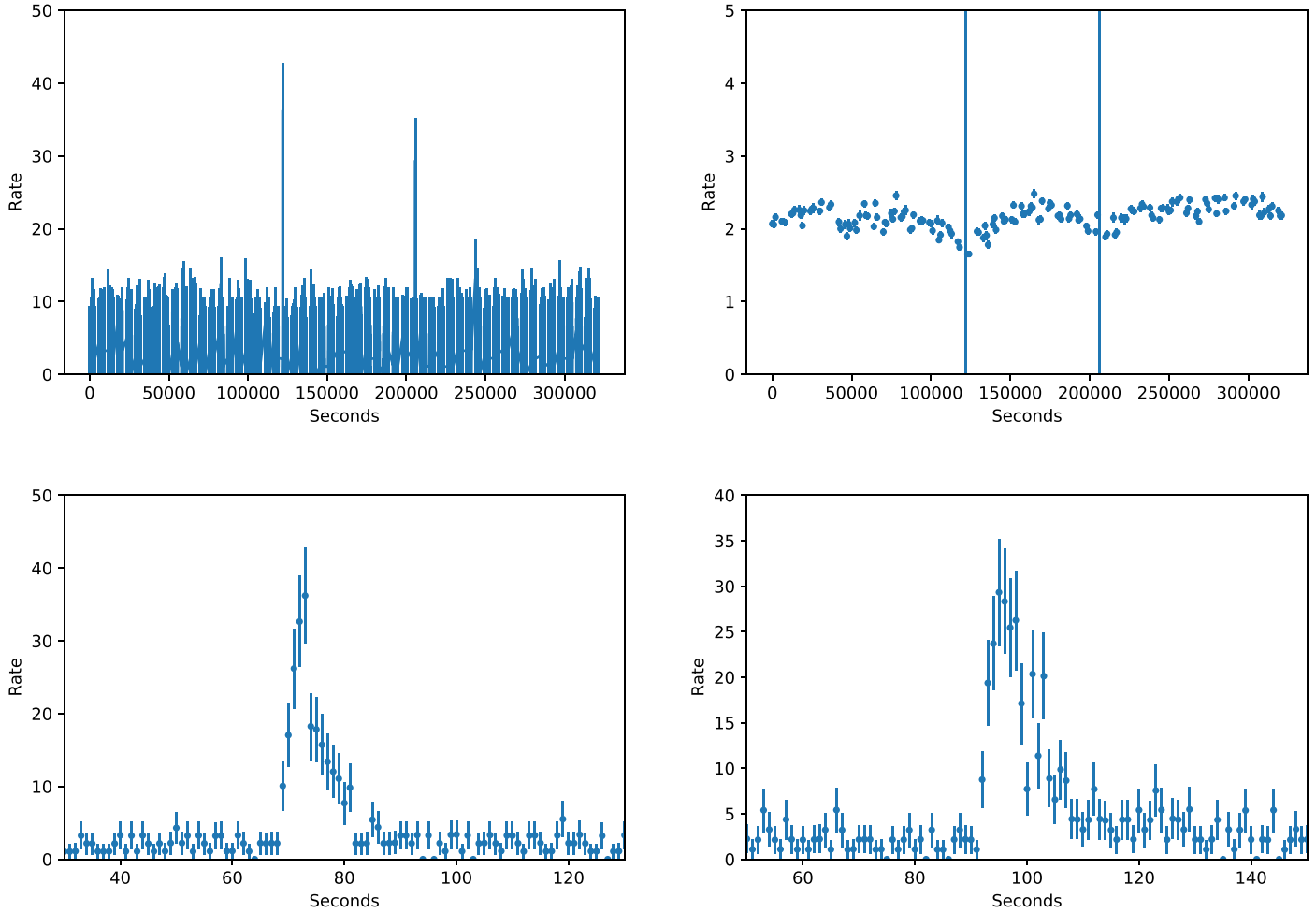

Figure 14. All panels show the 3–20 keV light curve of Obs. 7. (Top left) The full observation using 1 s bins clearly shows the two type I X-ray bursts. (Top right) Same data but using 1 ks bins. (Bottom panels) Zoomed-in view of the first (left) and second (right) type I X-ray burst.

Finally, our brief survey of the science potential from `StrayCats` observations shows the power of these observations. Through these highlights of a few selected observations, we have shown that these data can be used to track sources over long periods of time and provide a unique window into their behavior by providing improved sensitivity and finer spectral resolution compared to other all-sky monitors, such as MAXI and Swift-BAT.

This work was supported by the National Aeronautics and Space Administration (NASA) under grant No. 80NSSC19K1023 issued through the NNH18ZDA001N Astrophysics Data Analysis Program (ADAP). R.M.L. acknowledges the support of NASA through Hubble Fellowship Program grant HST-HF2-51440.001. R.A.K. acknowledges support from the Russian Science Foundation (grant 19-12-00396). J.H. acknowledges support from an appointment to the NASA Postdoctoral Program at the Goddard Space Flight Center, administered by the USRA through a contract with NASA.

Additionally, this work made use of data from the NuSTAR mission, a project led by the California Institute of Technology, managed by the Jet Propulsion Laboratory, and funded by the National Aeronautics and Space Administration. We thank the NuSTAR Operations, Software and Calibration teams for support with the execution and analysis of these observations. This research has made use of the NuSTAR Data Analysis Software (NuSTARDAS), jointly developed by the ASI Science Data Center (ASDC, Italy) and the California Institute of Technology (USA). This research has made use of data and/or software provided by the High Energy Astrophysics Science Archive Research Center (HEASARC), which is a service of the Astrophysics Science Division at NASA/GSFC.

Facilities: NuSTAR, Swift, MAXI, HEASARC.

Software: astropy (Robitaille et al. 2013; Astropy Collaboration et al. 2018), astroquery (Ginsburg et al. 2019), HEASoft/FTOOLS, IDL,[19] matplotlib (Hunter 2007), numpy,[20] pandas (Pandas Development Team 2020), plotly,[21] scikit-image,[22] Veusz.[23]

Appendix

The Appendix here contains an excerpt of the full StrayCats catalog (Table A1). The full version of the catalog will be available with the online version of the paper.

[19] https://www.harrisgeospatial.com/Software-Technology/IDL
[20] https://numpy.org
[21] https://plotly.com/python/
[22] https://scikit-image.org
[23] https://veusz.github.io

Table A1
`StrayCats` Excerpt

STRAYID	Classif.	SEQID	Mod.	Primary	TSTART	Exp.	SL Source	SL Type	$R.A._{SL}$	$Decl._{SL}$	$R.A._{Pri}$	$Decl._{Pri}$
StrayCatsI_0	Faint	30001014002	B	IC10_X1	56,967.8	88.47	NA	??	−999	−999	5.074	59.274
StrayCatsI_1	Unkn	90101010002	A	IGR_J00291p5934	57,231.5	38.10	NA	??	−999	−999	7.275	59.598
StrayCatsI_2	SL	90201030002	A	SWIFT_J003233d6m7306	57,586.7	54.92	SMC X-1	HMXB-NS	19.271	−73.443	8.197	−73.096
StrayCatsI_3	SL	90201041002	A	SMC_X3	57,704.7	38.60	SMC X-1	HMXB-NS	19.271	−73.443	13.030	−72.457
StrayCatsI_4	SL	30361002002	A	SXP_15d3	58,087.0	70.65	SMC X-1	HMXB-NS	19.271	−73.443	13.112	−73.373
StrayCatsI_5	SL	30361002004	A	SXP_15d3	58,418.9	58.35	SMC X-1	HMXB-NS	19.271	−73.443	13.141	−73.350
StrayCatsI_6	Faint	30361002004	B	SXP_15d3	58,418.9	58.13	NA	??	−999	−999	13.141	−73.350
StrayCatsI_7	Faint	50311003002	A	SMC_Deep_MOS03	57,876.1	172.39	NA	??	−999	−999	13.264	−72.488
StrayCatsI_8	SL	60301029006	A	IRAS_00521m7054	58,074.7	74.41	SMC X-1	HMXB-NS	19.271	−73.443	13.498	−70.667
StrayCatsI_9	SL	90101017002	A	SMC_X2	57,316.9	26.72	SMC X-1	HMXB-NS	19.271	−73.443	13.740	−73.707
StrayCatsI_10	SL	90102014004	A	SMC_X2	57,307.9	23.05	SMC X-1	HMXB-NS	19.271	−73.443	13.744	−73.695
StrayCatsI_11	SL	50311001002	B	SMC_Deep_MOS01	57,867.1	153.16	SMC X-1	HMXB-NS	19.271	−73.443	13.930	−72.439
StrayCatsI_12	SL	30202004006	B	SMC_X1	57,662.0	20.38	SMC X-3	HMXB-NS	13.023	−72.435	19.351	−73.462
StrayCatsI_13	SL	30202004002	A	SMC_X1	57,639.9	22.46	RX J0053.8–7226	HMXB-NS	13.480	−72.446	19.378	−73.442
StrayCatsI_14	SL	30202004002	B	SMC_X1	57,639.9	22.53	RX J0053.8–7226	HMXB-NS	13.480	−72.446	19.378	−73.442
StrayCatsI_15	SL	30202004004	B	SMC_X1	57,650.3	21.18	RX J0053.8–7226	HMXB-NS	13.480	−72.446	19.380	−73.454
StrayCatsI_16	SL	90001008002	A	GK_Per	57,116.1	42.35	NGC 1275	AGN	49.951	41.512	52.784	43.870
StrayCatsI_17	SL	30101021002	A	GK_Per	57,273.7	72.30	NGC 1275	AGN	49.951	41.512	52.812	43.933
StrayCatsI_18	SL	30101021002	B	GK_Per	57,273.7	72.16	NGC 1275	AGN	49.951	41.512	52.812	43.933
StrayCatsI_19	SL	10601407002	A	N132D	58,921.4	82.69	LMC X-2	LMXB-NS	80.117	−71.965	81.197	−69.695
StrayCatsI_20	SL	40101010002	B	N132D	57,366.2	68.85	LMC X-4	NS	83.206	−66.370	81.311	−69.666
StrayCatsI_21	SL	40101010002	B	N132D	57,366.2	68.85	LMC X-2	LMXB-NS	80.117	−71.965	81.311	−69.666
StrayCatsI_22	SL	30460020002	A	1RXS_J052523d2p241331	58,563.6	58.79	Crab	PWNe	83.633	22.015	81.316	24.192
StrayCatsI_23	SL	30460020002	B	1RXS_J052523d2p241331	58,563.6	58.29	Crab	PWNe	83.633	22.015	81.316	24.192
StrayCatsI_24	SL	30301014002	A	SGR_0526m66	58,156.9	47.03	LMC X-3	LMXB-BH	84.736	−64.084	81.500	−66.100
StrayCatsI_25	SL	30301014002	B	SGR_0526m66	58,156.9	46.90	LMC X-3	LMXB-BH	84.736	−64.084	81.500	−66.100

(This table is available in its entirety in FITS format.)

ORCID iDs

Brian W. Grefenstette https://orcid.org/0000-0002-1984-2932
Renee M. Ludlam https://orcid.org/0000-0002-8961-939X
Ellen T. Thompson https://orcid.org/0000-0002-3669-2294
Javier A. García https://orcid.org/0000-0003-3828-2448
Jeremy Hare https://orcid.org/0000-0002-8548-482X
Amruta D. Jaodand https://orcid.org/0000-0002-3850-6651
Roman A. Krivonos https://orcid.org/0000-0003-2737-5673
Kristin K. Madsen https://orcid.org/0000-0003-1252-4891
Guglielmo Mastroserio https://orcid.org/0000-0003-4216-7936
Catherine M. Slaughter https://orcid.org/0000-0002-5752-3780
John A. Tomsick https://orcid.org/0000-0001-5506-9855
Daniel Wik https://orcid.org/0000-0001-9110-2245
Andreas Zoglauer https://orcid.org/0000-0001-9067-3150

References

Arnaud, K. A. 1996, adass V, 101, 17
Astropy Collaboration, Price-Whelan, A. M., Sipőcz, B. M., et al. 2018, AJ, 156, 123
Belloni, T., Klein-Wolt, M., Méndez, M., van der Klis, M., & van Paradijs, J. 2000, A&A, 355, 271
Castro-Tirado, A. J., Brandt, S., & Lund, N. 1992, IAUC, 5590, 2
Chenevez, J., Galloway, D. K., in'tZ, J. J. M., et al. 2016, ApJ, 818, 135
Coughenour, B. M., Cackett, E. M., Miller, J. M., & Ludlam, R. M. 2018, ApJ, 867, 64
Gehrels, N., Chincarini, G., Giommi, P., et al. 2004, ApJ, 611, 1005
Ginsburg, A., Sipőcz, B. M., Brasseur, C. E., et al. 2019, AJ, 157, 98
Harrison, F. A., Craig, W. W., Christensen, F. E., et al. 2013, ApJ, 770, 103
Hasinger, G., & van der Klis, M. 1989, A&A, 225, 79
Houck, J. C., & Denicola, L. A. 2000, in ASP Conf. Ser. 216, Astronomical Data Analysis Software and Systems IX, ed. N. Manset, C. Veillet, & D. Crabtree (San Francisco, CA: ASP), 591
Hunter, J. D. 2007, CSE, 9, 90
Huppenkothen, D., Bachetti, M., Stevens, A. L., et al. 2019, ApJ, 881, 39
Krivonos, R., Revnivtsev, M., Churazov, E., et al. 2007, A&A, 463, 957
Krivonos, R., Tsygankov, S., Lutovinov, A., et al. 2012, A&A, 545, A27
Lin, D., Remillard, R. A., & Homan, J. 2007, ApJ, 667, 1073
Ludlam, R. M., Miller, J. M., Barret, D., et al. 2019, ApJ, 873, 99
Madsen, K. K., Christensen, F. E., Craig, W. W., et al. 2017a, JATIS, 3, 044003
Madsen, K. K., Forster, K., Grefenstette, B. W., Harrison, F. A., & Stern, D. 2017b, ApJ, 841, 56
Matsuoka, M., Kawasaki, K., Ueno, S., et al. 2009, PASJ, 61, 999
McClintock, J. E., Shafee, R., Narayan, R., et al. 2006, ApJ, 652, 518
Miller, J. M., Raymond, J., Fabian, A. C., et al. 2016, ApJL, 821, L9
Miller, J. M., Zoghbi, A., Raymond, J., et al. 2020, ApJ, 904, 30
Neilsen, J., Cackett, E., Remillard, R. A., et al. 2018, ApJL, 860, L19
Neilsen, J., Homan, J., Steiner, J. F., et al. 2020, ApJ, 902, 152
Oh, K., Koss, M., Markwardt, C. B., et al. 2018, ApJS, 235, 4
Pandas Development Team, T.P. 2020, Pandas-Dev/Pandas: Pandas v1.1, Zenodo, doi:10.5281/zenodo.3509134
Robitaille, T. P., Tollerud, E. J., Greenfield, P., et al. 2013, A&A, 558, A33
Seifina, E., & Titarchuk, L. 2012, ApJ, 747, 99
Strohmayer, T. E., Gendreau, K. C., Altamirano, D., et al. 2018, ApJ, 865, 63
Ubertini, P., Bazzano, A., Cocchi, M., et al. 1999, ApJL, 514, L27
Wik, D. R., Hornstrup, A., Molendi, S., et al. 2014, ApJ, 792, 48
Winkler, C., Courvoisier, T. J.-L., Di Cocco, G., et al. 2003, A&A, 411, L1
Zoghbi, A., Miller, J. M., King, A. L., et al. 2016, ApJ, 833, 165